Confined Volume Change in Sn-Co-C Ternary Tube-in-Tube Composites for High-Capacity and Long-Life Lithium Storage

*Yan Gu, Fendan Wu, and Yong Wang**

All high capacity Li-alloy anodes for Li-ion battery suffer from enormous volume expansion and extraction during the lithium-ion insertion and extraction process. A Sn-Co-CNT@CNT ternary tube-in-tube nanostructure is prepared by an in situ template technique and shows perfect structure suitability to solve the critical volume change problem. The morphology, size, and quantity of the filled CNT-supported Sn-Co nanoparticles can be also tuned by adjusting the experimental conditions to achieve optimal electrochemical performances. The tube-in-tube product exhibits larger-than-theoretical reversible capacities of 890–811 mA h g^{-1} at 0.1C in 200 cycles and excellent rate capability and high-rate cycling stability. The excellent electrochemical performance is mainly attributed to the confined volume change in the nanotube cavities and ensured permanent electrical connectivity of the immobilized Sn-Co anodes.

1. Introduction

Lithium-ion batteries have attracted great interest as the power sources for portable electronic devices and electrical vehicles, and for potential large-scale electricity storage. It is highly desirable that the next-generation electrode materials can deliver high energy density, long cycle life, and stable high-rate performance. Sn-based anode materials have been extensively studied, since Sn exhibits a larger theoretical capacity (≈990 mA h g^{-1}) than commercial graphite anodes (372 mA h g^{-1}).[1–4] However, its commercial application is prevented by fast capacity fading during cycling. This has been ascribed to the large volume change associated with the lithium insertion and extraction process into Sn electrodes, which would lead to the loss of the electrical contact of Sn materials and subsequently their lithium-storage capacity.[3] The capacity fading induced by a large volume change is also a critical problem for other high-capacity materials such as Si, Sb, Al, and transition metal oxides.[3,5–11] To overcome the problem, Sn-based composite anodes are often introduced, such as Sn-Co-C,[12–25] which was triggered by the announcement of Sony's commercial Sn-Co-C anodes. Commercial Sn-Co-C anodes have been examined carefully, and stable reversible capacities of ≈400–450 mA h g^{-1} have been achieved in 30 cycles.[24,25] However, this capacity is still limited and cannot meet the requirements of next-generation electrodes for Li-ion batteries.

Herein, a new hierarchical tube-in-tube nanostructure, namely Sn-Co-CNT@CNT, is reported in this work. **Scheme 1** shows a schematic illustration of lithium storage in this electrode. The volume change of the Sn-Co particles is confined inside the CNT cavities and the Sn-Co particles can, in principal, be assured to be electrically connected by the presence of the filled small CNTs and external large CNT wrapping. This tube-in-tube nanostructure showed highly reversible large capacities at both small and high currents (890 mA h g^{-1} at 99 mA g^{-1} and 557 mA h g^{-1} at 4950 mA g^{-1}) when tested as anode materials for rechargeable lithium-ion batteries.

2. Results and Discussion

The crystallographic structure of the product was analyzed by X-ray powder diffraction (XRD), as shown in **Figure 1**a. A few weak characteristic peaks at 30.6°, 32.0°, 43.9°, 44.9° could be indexed to the (200), (101), (220), and (211) planes of tetragonal Sn (PDF 04-0673, lattice constants: a_0 = 5.83 Å, c_0 = 3.18 Å), respectively. The peak at 43.2° was assigned to the (602) crystalline plane of orthorhombic $CoSn_3$ (PDF 48-1813). It is noted that, although this peak at ≈43.2° may be assigned to either $CoSn_3$ or Co_3Sn_2, the former is more possible because an excessive amount of Sn (molar ratio of Sn:Co = 5:1) was used in the preparation process. The broad diffraction peak at around 25° was attributed to the (002) plane of carbon. Field-emission scanning electron microscopy (FE-SEM) images (Figure 1b,c) show the as-prepared Sn-Co-CNT@CNT nanostructure (Sample A, molar ratio of Sn:Co = 5:1). A large amount of 1D nanostructures could be observed with uniform diameters of ≈180–250 nm, which is in a good agreement with the pore size of the alumina membrane. A thin CNT layer has been demonstrated to be formed by the catalysis decomposition of acetylene and its deposition on alumina pore walls.[26,27] As shown in the top-view image of the products (Figure 1c), some filler materials were found inside the open-ended carbon nanotubes.

The transmission electron microscopy (TEM) images in **Figure 2**a,b confirm the tube-in-tube filling nanostructure. A

Y. Gu, F. Wang, Prof. Y. Wang
Department of Chemical Engineering
School of Environmental and Chemical Engineering
Shanghai University
Shangda Road 99, Shanghai, P. R. China, 200444
E-mail: yongwang@shu.edu.cn

DOI: 10.1002/adfm.201202136

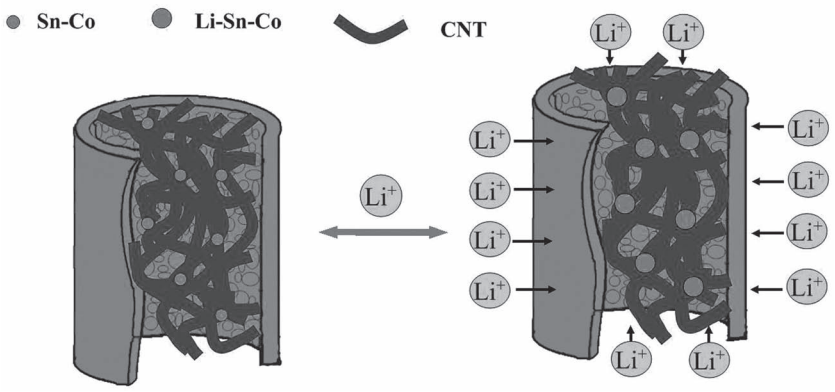

Scheme 1. Schematic showing the confined volume change during the lithium insertion and extraction process in a Sn-Co-CNT@CNT anode.

large number of small CNT-supported Sn-Co nanoparticles were encapsulated completely in the hollow cavities of the large CNTs (≈200 nm), and there were no Sn-Co materials observed on the exterior surface of the large CNTs. These encapsulated small CNTs were ≈25 nm in diameter and a few hundred nanometers in length. The corresponding energy-dispersive X-ray spectroscopy (EDS) is shown in Figure 2e, which reveals the presence of Sn and Co elements in the Sn-Co-CNT@CNT nanostructure. The carbon content was determined by the CHN elemental analysis to be ≈50.1 wt% in the composite, suggesting that the Sn-Co alloy is a highly efficient catalyst for promoting the growth of a large quantity of small-diameter CNTs inside the 200 nm CNTs. To get further insight into the structural features, high-resolution (HR-TEM) images of the large CNTs and the filled, small CNTs are shown in Figure 2c and 2d, respectively. The external, large CNT shell was made of staggered and short-range graphene nanosheets with a thickness of ≈5–8 nm. The nearly triangular tip opening of a filled small CNT is shown clearly in Figure 2d. These encapsulated small CNTs and large host CNTs (≈200 nm in diameter) are both largely amorphous, which may offer convenient lithium diffusion routes through the CNT walls and more active sites for lithium storage.[28–32]

The TEM images in **Figure 3**a,b show the Sn-Co-CNT@CNT products (sample B, 65.8 wt% Sn, molar ratio of Sn:Co = 5:1) prepared from a high precursor concentration ($SnCl_4$:$CoCl_2$ = 5 M: 1 M). Induced by more Sn-Co materials, 200 nm CNTs were filled with a large quantity of Sn-Co-CNT materials in their cavities. These Sn-Co nanoparticles were still below 10 nm in size. A small open-ended CNT is stretched out as shown in Figure 3b. The TEM images in Figure 3c,d show the product prepared from a lower precursor concentration (Sample C ($SnCl_4$:$CoCl_2$ = 0.4 M:0.08 M). A number of CNTs (≈15–20 nm in diameter) with triangular tip openings were found to be encapsulated completely in a large CNT. Therefore the filled Sn-Co-CNT quantity could be tuned by adjusting the usage amount of Sn-Co precursors, which are the catalyst for the growth of filled CNTs.

On the basis of the above observations, the growth process of a Sn-Co-CNT@CNT tube-in-tube composite is suggested in Figure 3e. $SnCl_4$ and $CoCl_2$ are reduced to Sn-Co alloy by acetylene gas, which is subsequently used as the in situ catalyst to decompose the acetylene gas and promote the formation of small CNTs inside the alumina pores. On the other hand, during the flowing process of C_2H_2, the catalytic action of the alumina walls leads to the formation of a thin CNT layer around alumina pore walls. As a result, Sn-Co-CNTs composites are completely encapsulated inside these CNT-coated alumina pores. These alumina templates can be easily removed by immersing the membranes in NaOH solution and the Sn-Co-CNT@CNT nanostructure was obtained as the final product. It was found that $SnCl_4$ and $CoCl_2$ could be readily reduced by C_2H_2 to Sn-Co particles. Due to the low melting point of the Sn-Co particles (Sn melting point = 232 °C), these Sn-Co particles would be melt and are easy to aggregate, forming very large particles. The TEM image in **Figure 4**a shows the Sn-Co-CNT@CNT nanostructure prepared directly from $SnCl_4$ and $CoCl_2$ without pre-heating at 650 °C in air. The resulting large Sn-Co particles can also promote CNT growth. As shown in Figure 4a, a large-diameter CNT is obtained because its diameter is largely determined by the particle size of the Sn-Co catalyst, based on the growth mechanism of the metal-catalyzed chemical vapor deposition (CVD) process. To avoid this unfavorable phenomenon, a process of pre-heating in air has to be used to form tin oxide and cobalt oxide before the CVD reaction. It is believed that the kinetics of the reduction process from metal oxides are slowed down compared with the process from $SnCl_4$ and $CoCl_2$. Therefore, there is enough time for the in situ catalytic formation of CNTs, which would subsequently support Sn-Co particles and prevent their particle-size growth. As a result, Sn-Co nanoparticles, supported on small CNTs, could be successfully filled inside a large CNT as shown in the previous Figure 1–3. The intermediate tin oxide-cobalt oxide nanotubular products are shown in the SEM image of Figure 4b and the TEM image of Figure 4c. Sn-Co-O nanotubes are composed of numerous Sn-Co-O nanoparticles with particle sizes below 10 nm. The X-ray diffraction patterns of the Sn-Co-O intermediate products are also shown in Figure 4d. All of the peaks in the product can be indexed into the mixture of SnO_2 (PDF 41-1445) and Co_3O_4 (PDF 42-1467).

It is noted that a large quantity of small CNTs are grown further by the filled Sn-Co particles inside a large CNT in this work and form the complex Sn-Co-CNTs@CNT tube-in-tube structure. This is the unique difference compared with previous CNT encapsulation composites, in which nanoparticles are usually obtained.[29,31,33] The melted Sn or Sn-Sb with a low melting point has also been reported to be encapsulated inside the hard template of a CNT, thus forming a rod-like morphology.[32,34] These filled small CNTs are highly desired for property improvement because they are able to immobilize the Sn-Co particles inside the large CNT and improve their electrical contact and mechanical stability during repetitive cycling with lithium ions. The electrochemical performance of Sn-Co-CNT@CNT anodes (Sample A and Sample B) was tested in laboratory-type lithium cells and the results tested at a current of 0.1C (1C = 990 mA g^{-1}, ≈2 mg cm^{-2}) are shown in **Figure 5**.

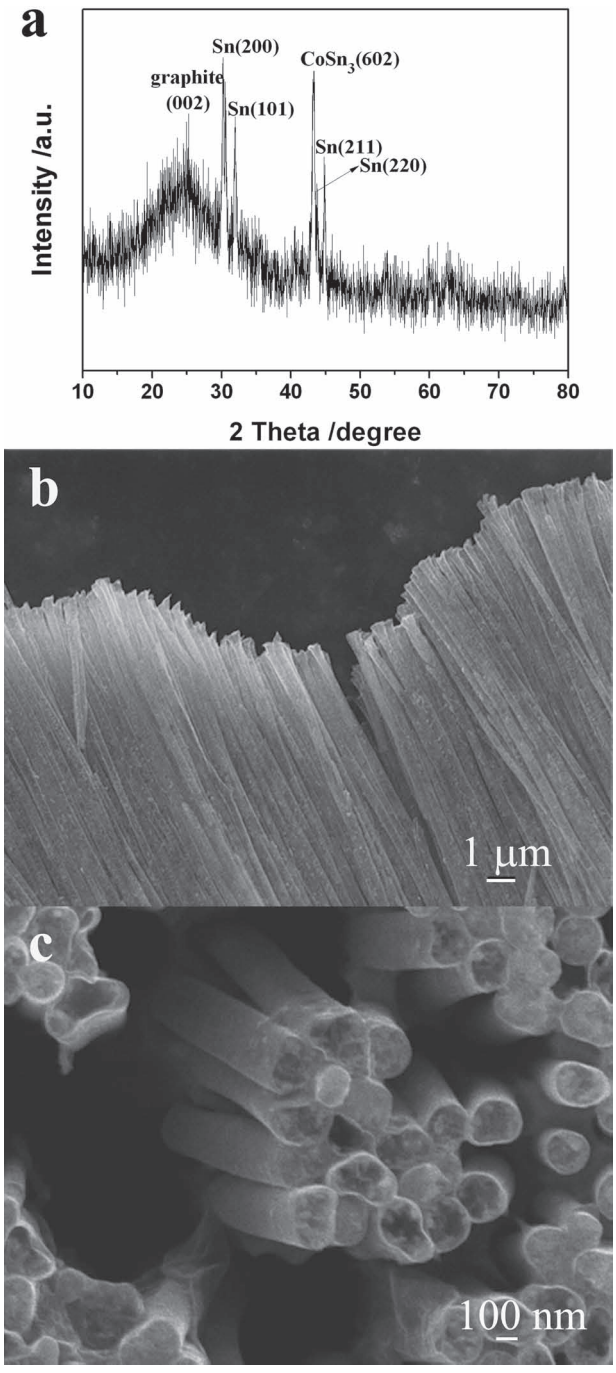

Figure 1. Sn-Co-CNT@CNTs. a) The X-ray powder diffraction (XRD) pattern. b) Side-view SEM image. c) Top-view SEM image.

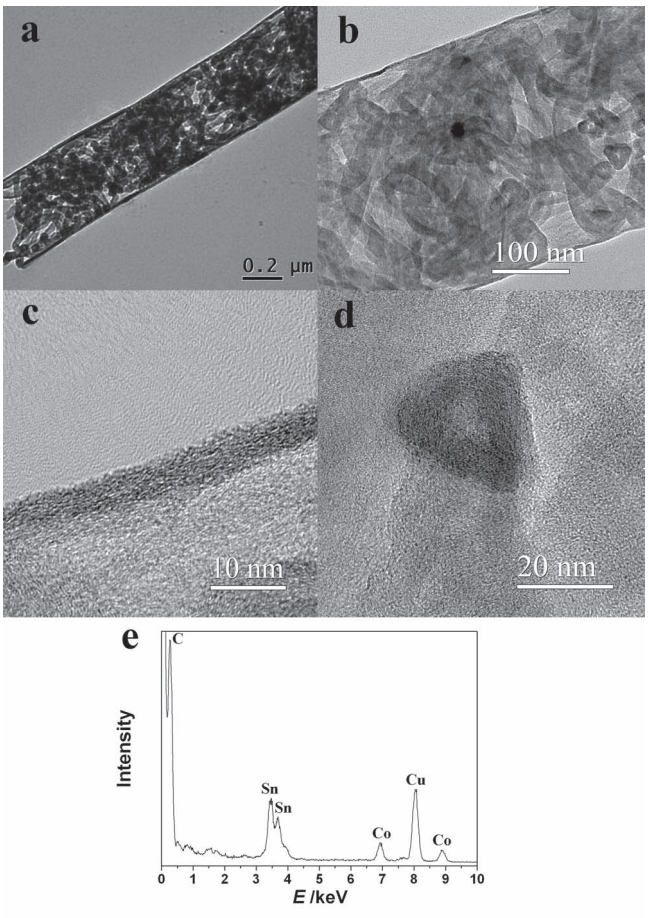

Figure 2. Sn-Co-CNT@CNTs. a,b) TEM images. c,d) HR-TEM images showing: c) the large CNT wall and d) the tip opening of a filled small CNT. e) The EDS spectrum.

The highly homogeneous electrode slurry was obtained using a high-speed homogenizer, which is suitable for handling a small amount of electrode material prepared by the templated method (the minimum treatment volume is 0.2 mL). The initial discharge (lithium insertion) and charge (lithium extraction) capacities of sample A were 1686 and 890 mA h g^{-1} respectively. The initial capacity loss should be mainly ascribed to the lithium-ion consumption in the electrolyte decomposition and the formation of a solid electrolyte interface (SEI) film, which is inevitable for most nanoscale electrode materials with large surface areas.[2–11] This weakness of nanoscale electrodes could be improved by material pretreatment, such as by pre-lithiation.[2] The reversible charge capacity (890 mA h g^{-1}) is much higher than the theoretical capacity value (636 mA h g^{-1}) based on the weighted sum of three components (45.4 wt% of Sn, theoretical capacity: 990 mA h g^{-1}; 50.1 wt% of carbon, theoretical capacity: 372 mA h g^{-1}, and 4.5 wt% of inactive Co). It is noted that the reversible capacity (890 mA h g^{-1}) is also substantially larger than that of our previous CNT-encapsulated SnO_2 composite (585 mA h g^{-1}) with higher Sn loading (73.3 wt% SnO_2).[26] The introduction of the Co element in this work promotes the growth of numerous, filled small CNTs inside a large CNT. Moreover, Co doping has been explored as a useful strategy for improving the mechanical stability and electrochemical performance of Sn materials upon cycling.[12–25] Although the mechanism for extremely high capacity is not very clear, it is believed that this large capacity should be mainly ascribed to more active sites associated with the disordered small CNTs and porous spaces among packed Sn-Co-CNT materials inside the large CNT.[28,35,36] Li-ion storage has also been suggested by a possible Faradaic capacitance effect of carbonaceous

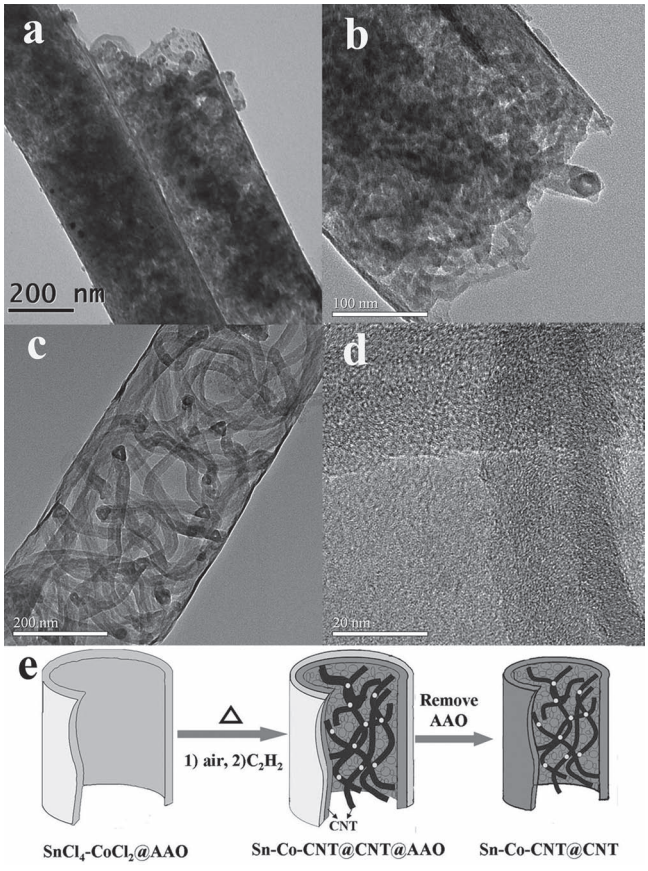

Figure 3. a–d) TEM images showing Sn-Co-CNT@CNT prepared from a higher precursor concentration (a,b) and a lower precursor concentration (c,d). e) schematic illustration showing the growth process of the Sn-Co-CNT@CNT nanostructure.

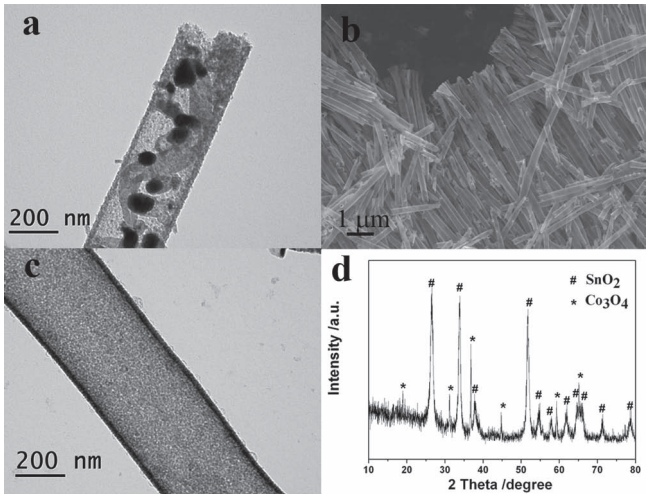

Figure 4. a) TEM image of the Sn-Co-CNT@CNT nanostructure prepared directly from $SnCl_4$ and $CoCl_2$ without pre-heating at 650 °C in air. b,c) SEM and TEM images of the intermediate Sn-Co-O nanotube products. d) The X-ray powder diffraction (XRD) pattern of the intermediate Sn-Co-O nanotube products.

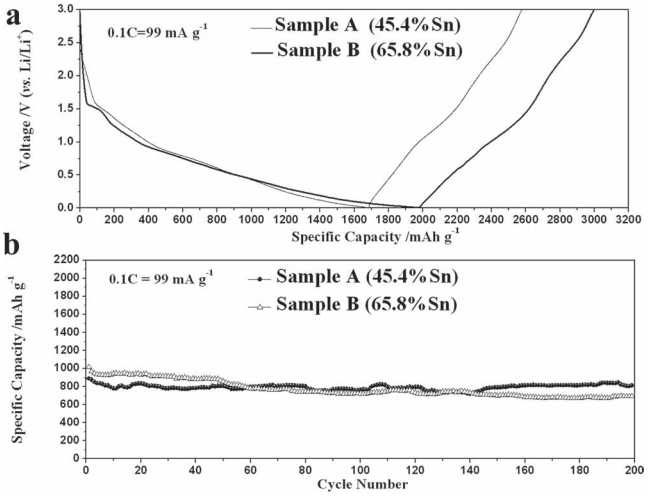

Figure 5. Electrochemical properties of the Sn-Co-CNT@CNT nanostructure. a) The first-cycle discharge (lithium insertion) and charge (lithium extraction) curves. b) Cycling performances at 0.1C, 1C = 990 mA g^{-1}.

materials.[37] Notably, although a larger capacity has been reported for previous disordered carbon anodes compared with graphite anodes, a poor capacity retention has also been observed for these disordered carbon anodes.[28] To achieve a high capacity with good cyclability is still a big challenge.

The cycling performance of Sn-Co-CNT@CNT (Sample A and B) at 0.1C is shown in Figure 5b. These tube-in-tube nanostructures exhibited excellent cycling performances with Li-ion storage capacities maintained at a high level. The charge capacity of sample A decreased from an initial 890 mA h g^{-1} to 811 mA h g^{-1} after 200 cycles, which still corresponds to 91.1% of the initial charge capacity. The average capacity fading is only 0.044% capacity loss per cycle, which is comparable with that of commercial graphite anodes. In comparison, previous CNT-encapsulated SnSb nanorods exhibited a fast capacity fading from an initial 948 mA h g^{-1} to 680 mA h g^{-1} in 80 cycles.[34] This fading rate is ≈8 times faster than that of the Sn-Co-CNT@CNT structure. Smaller reversible capacities have also been observed for CNT-encapsulated SnO_2 (585 mA h g^{-1} after 200 cycles)[26] and Sn nanoparticles (474 mA h g^{-1} after 80 cycles)[29] anodes under similar test conditions. Therefore, the tube-in-tube nanostructure is found to be better suitable to solving the critical volume change problem compared with other CNT-encapsulation structures. Notably, the remaining reversible capacity (811 mA h g^{-1} for sample A) after long 200 cycles is still more than 2 times as large as the theoretical value of commercial graphite (372 mA h g^{-1}) and much higher than the theoretical values of the Sn-Co-C composite (636 mA h g^{-1}) and the commercial Sn-Co-C composite anodes (≈450–400 mA h g^{-1} in 30 cycles).[24,25] This large reversible capacity after 200 cycles has not been witnessed in all previous Sn-Co-C[12–25] or Sn-CNT composites.[29–34]

To further attest the merits of the tube-in-tube structure electrodes, the electrochemical performances of sample A at high current rates were explored and are shown in **Figure 6**a and 6c. The loading amount of the electrode was kept at ≈2 mg cm^{-2} and the thickness of the electrode materials was kept at

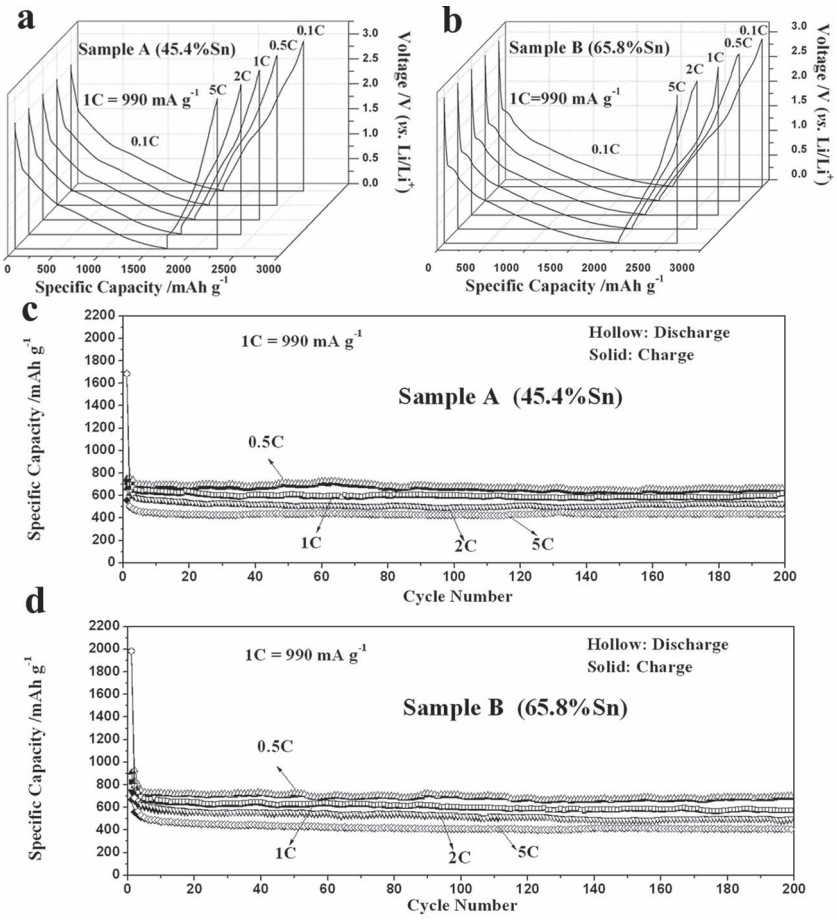

Figure 6. Electrochemical properties of Sn-Co-CNT@CNT anodes (Sample A and B) at large currents. a,b) the first-cycle discharge (lithium insertion) and charge (lithium extraction) curves. c,d) Cycling performances.

≈20 μm. The initial charge capacities were 751, 714, 664, and 557 mA h g^{-1} at various currents of 495 mA g^{-1} (0.5 C), 990 mA g^{-1} (1C), 1980 mA g^{-1} (2C), and 4950 mA g^{-1} (5C), respectively. The high-rate cycling performance was also very stable. For instance, a reversible charge capacity of 612 mA h g^{-1} was retained after 200 cycles at 1C, which amounted to 85.7% of the initial charge capacity. These excellent high-rate electrochemical performances have not been reported previously in Sn-Co-C[12–25] or Sn-CNT composites.[29–34] The electrochemical properties of sample B at various currents are compared in Figure 6b and 6d. Compared to sample A, sample B exhibited larger capacities, but slightly worse cycling stabilities at both small and high currents. For example, its initial charge capacity was 1015 mA h g^{-1} at 0.1C, which decreased to 692 mA h g^{-1} after 200 cycles. This experimental result should be mainly ascribed to the presence of more Sn materials in sample B (65.8 wt% Sn) compared with Sample A (45.4 wt% Sn). The pristine Sn material has a larger Li-ion storage capacity than carbon, but a worse cycling performance.[3]

The excellent electrochemical properties of the Sn-Co-CNT@CNT tube-in-tube composite should be largely attributed to the unique structure-associated merits. Sn-Co alloy particles are deposited on small CNTs and the resulting Sn-Co-CNT composites are completely filled inside a large CNT. Distinguished from previous CNT-encapsulated electrodes,[29–34] the introduction of elemental Co leads to a growth of numerous small CNTs inside the large CNT, in this work. These small CNTs substrate could function as a skeleton to link these Sn-Co particles and improve their electrical contact and mechanical stability during the volume expansion of the Li-ion insertion process. An external, large CNT skin provides a perfect "barrier" to confine the volume change and immobilize these Sn-Co particles and small CNTs further. Even if particle cracking is still possible and some Sn-Co particles are detached from the small CNTs surfaces, these encapsulated particles would be captured by other CNTs, thus ensuring a permanent electrical connectivity of Sn-Co anodes with CNTs and the current collector. Moreover, the void spaces among packed Sn-Co-CNTs inside the large CNT may provide more active sites for Li-ion storage. More importantly, these porous spaces are very helpful in accommodating the local volume change of Sn-Co anode materials and promote a fast diffusion of lithium ions and electrolytes. This is a key factor to a high-rate electrochemical performance.[38] The TEM image of the Sn-Co-CNT@CNT composite anode after 200 cycles at 1C is shown in **Figure 7**. In the presence of carbon black and binder, 1D nanotube-like nanostructures could be retained, which confirms the stable anode structure in the repetitive lithium-insertion and extraction process. The external CNT exhibited a larger diameter of ≈300 nm compared with the initial value (≈180–250 nm) before cycling. This

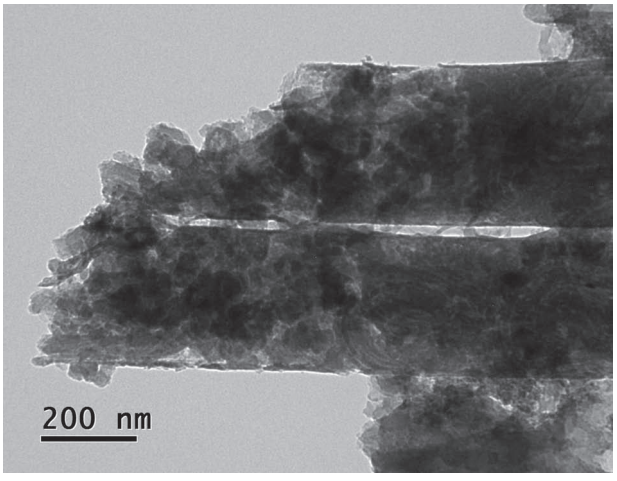

Figure 7. The TEM image shows Sn-Co-CNT@CNT anode materials after 200 cycles at 1C in the presence of carbon black and PVDF binder materials.

may be ascribed to confined volume expansion of the Li-Sn-Co materials inside the flexible CNT.

3. Conclusions

In conclusion, a new Sn-Co-CNT@CNT tube-in-tube nanostructure was designed and synthesized in this work. Interestingly, a large amount of small CNTs were filled inside a large CNT by the catalytic action of the filled Sn-Co particles. The morphology, size and quantity of the filled Sn-Co-CNT composite could be also easily tuned. When investigated as anode materials for secondary lithium-ion batteries, this Sn-Co-CNT@CNT tube-in-tube nanostructure showed an unprecedented highly reversible capacity at both small and large current rates in 200 cycles among all relative Sn-Co-C or Sn-CNT anode materials. The tube-in-tube growth and Li-storage mechanisms for Sn-Co-CNT@CNT nanostructures and the superior electrochemical performance were also discussed and suggested.

4. Experimental Section

Synthesis of Sn Co CNT@CNTs: All of the reagents were of analytical grade and used without further treatment. In a typical experiment for sample A, certain amounts of $SnCl_4{\cdot}5H_2O$ and $CoCl_2{\cdot}6H_2O$ were added into ethanol (10 mL) under vigorous stirring to achieve a transparent precursor solution containing $SnCl_4$ (1 M) and $CoCl_2$ (0.2 M). Anodic aluminum oxide (AAO) (Whatman, Anodisc, ϕ = 200 nm) membranes were immersed in water for 30 min to remove air bubbles in the pores and then equilibrated in the above precursor solution for 5 h. The membranes were dried at 80 °C for 2 h to evaporate ethanol solvent in the impregnated membranes and a thin film of liquid $SnCl_4$ (melting point: –33 °C) and solid $CoCl_2$ was formed on the inner pore walls of the AAO membranes. The membranes were then calcined in air at 650 °C for 10 h to obtain tin oxide/cobalt oxide-filled AAO membranes. These membranes were then heated up in a tubular furnace at 550 °C under a flowing gas mixture of C_2H_2 (5%) and N_2 (95%) at a rate of 100 sccm. The furnace was cooled down to room temperature in pure N_2. The surfaces of the as-obtained membranes were polished gently with sandpaper and immersed in a NaOH (2 M) aqueous solution to remove the template. A black powder was obtained as sample A after copious washing with deionized water and drying at 130 °C in vacuum. Sample B and sample C were similarly prepared by impregnating AAO membranes with the precursor's ethanol solutions with $SnCl_4$:$CoCl_2$ = 5 M:1 M or 0.4 M:0.08 M.

Materials Characterization: The as-prepared products were characterized by powder XRD (Rigaku D/max-2550V, CuK_α radiation), FE-SEM/energy-dispersive X-ray spectroscopy (EDS) (JSM-6700F), TEM/selected area electron diffraction (SAED)/EDS (JEOL JEM-200CX and JEM-2010F), and elemental analysis (VARIO EL111).

Preparation of Electrodes and Electrochemical Measurements: The electrode slurry was obtained using a high-speed homogenizer (Scientz S10, 8000–30 000 rpm, 0.2–120 mL). The working electrodes were composed of 80 wt% active materials, 10 wt% carbon black (conductivity agent) and 10 wt% poly(vinylidene difluoride) (PVDF) (binder). Lithium foils were used as the counter and reference electrodes. The electrolyte was $LiPF_6$ (1 M) in a 1:1 w/w mixture of ethylene carbonate and dimethyl carbonate. The cells were assembled in an argon-filled glove box. The discharge (lithium insertion) and charge (lithium extraction) tests were performed using a LAND-CT2001 test system at a constant current of 99 mA g^{-1} (0.1C, 1C = 990 mA g^{-1}) in the fixed voltage range of 5 mV–3.0 V. The loading amount of the electrode was kept at ≈2 mg cm^{-2}. The thickness of the electrode materials was ≈20 μm. Higher currents of 495 mA g^{-1} (0.5C), 990 mA g^{-1} (1C), 1980 mA g^{-1} (2C), and 4950 mA g^{-1} (5C) were also used and the first-cycle discharge were all kept at 0.1C. Cyclic voltammetry (CV) was carried out using a CH Instruments electrochemical workstation (model 660D) at a scanning rate of 0.05 mV s^{-1}.

Acknowledgements

The authors gratefully acknowledge financial support from the Program for Professor of Special Appointment (Eastern Scholar), the National Natural Science Foundation of China (51271105, 50971085) and the Shanghai Municipal Government (11JC1403900, 11SG38, S30109).

Received: July 29, 2012
Published online: September 24, 2012

[1] P. G. Bruce, J. Hassoun, Y. K. Sun, *Energy Environ. Sci.* **2011**, *4*, 3287–3295.
[2] P. Verma, P. Maire, P. Novak, *Electrochim. Acta* **2010**, *55*, 6332–6341.
[3] C. M. Park, J. H. Kim, H. Kim, H. J. Sohn, *Chem. Soc. Rev.* **2010**, *39*, 3115–3141.
[4] X. F. Li, X. B. Meng, J. Liu, D. S. Geng, Y. Zhang, M. N. Banis, Y. L. Li, J. L. Yang, R. Y. Li, X. L. Sun, M. Cai, M. W. Verbrugge, *Adv. Funct. Mater.* **2012**, *8*, 1647–1654.
[5] Z. Y. Zhou, N. Tian, J. T. Li, I. Broadwell, S. G. Sun, *Chem. Soc. Rev.* **2011**, *40*, 4167–4185.
[6] Z. Y. Wang, D. Luan, F. Y. C. Boey, X. W. Lou, *J. Am. Chem. Soc.* **2011**, *133*, 4738–4741.
[7] D. Y. Chen, X. Mei, G. Ji, M. H. Lu, J. P. Xie, J. M. Lu, J. Y. Lee, *Angew. Chem. Int. Ed.* **2012**, *51*, 2409–2413.
[8] J. L. Goldman, B. R. Long, A. A. Gewirth, R. G. Nuzzo, *Adv. Funct. Mater.* **2011**, *13*, 2412–2422.
[9] B. M. Bang, H. Kim, J. P. Lee, J. Cho, S. Park, *Energy Environ. Sci.* **2011**, *4*, 3395–3399.
[10] J. C. Guo, Q. Liu, C. S. Wang, M. R. Zachariah, *Adv. Funct. Mater.* **2012**, *4*, 803–811.
[11] J. L. Goldman, B. R. Long, A. A. Gewirth, R. G. Nuzzo, *Adv. Funct. Mater.* **2011**, *13*, 2412–2422.
[12] M. Y. Li, C. L. Liu, M. R. Shi, W. S. Dong, *Electrochim. Acta* **2011**, *56*, 3023–3028.
[13] P. P. Ferguson, A. D. W. Todd, J. R. Dahn, *Electrochem. Commun.* **2010**, *12*, 1041–1044.
[14] L. Huang, J. S. Cai, Y. He, F. S. Ke, S. G. Sun, *Electrochem. Commun.* **2009**, *11*, 950–953.
[15] P. P. Ferguson, M. L. Martine, A. E. George, J. R. Dahn, *J. Power Sources* **2009**, *194*, 794–800.
[16] Z. X. Chen, J. F. Qian, X. P. Ai, Y. L. Cao, H. X. Yang, *J. Power Sources* **2009**, *189*, 730–732.
[17] S. I. Lee, S. Yoon, C. M. Park, J. M. Lee, H. Kim, D. Im, S. G. Doo, H. J. Sohn, *Electrochim. Acta* **2008**, *54*, 364–369.
[18] P. P. Ferguson, A. D. W. Todd, J. R. Dahn, *Electrochem. Commun.* **2008**, *10*, 25–31.
[19] J. Hassoun, G. Mulas, S. Panero, B. Scrosati, *Electrochem. Commun.* **2007**, *9*, 2075–2081.
[20] J. Hassoun, S. Panero, G. Mulas, B. Scrosati, *J. Power Sources* **2007**, *171*, 928–931.
[21] G. F. Ortiz, R. Alcántara, I. Rodríguez, J. L. Tirado, *J. Electroanal. Chem.* **2007**, *605*, 98–108.
[22] R. B. Lewis, A. Timmons, R. E. Mar, J. R. Dahn, *J. Electrochem. Soc.* **2007**, *154*, A213–A216.
[23] A. D.W. Todd, R. E. Mar, J. R. J. Dahn, *Electrochem. Soc.* **2007**, *154*, A597–A604.

[24] Q. Fan, P. J. Chupas, M. S. Whittingham, *Electrochem. Solid-State Lett.* **2007**, *10*, A274–A278.
[25] R. Zhang, M. S. Whittingham, *Electrochem. Solid-State Lett.* **2010**, *13*, A184–A187.
[26] Y. Wang, H. C. Zeng, J. Y. Lee, *Adv. Mater.* **2006**, *18*, 645–649.
[27] G. Che, B. B. Lakshmi, E. R. Fisher, C. R. Martin, *Nature* **1998**, *393*, 346–349.
[28] N. A. Kaskhedikar, J. Maier, *Adv. Mater.* **2009**, *21*, 2664–2680.
[29] Y. Wang, M. H. Wu, Z. Jiao, J. Y. Lee, *Chem. Mater.* **2009**, *21*, 3210–3215.
[30] Y. Q. Zou, Y. Wang, *ACS Nano* **2011**, *5*, 8108–8114.
[31] M. F. Ng, J. W. Zheng, P. Wu, *J. Phys. Chem. C* **2010**, *114*, 8542–8545.
[32] R. Y. Li, X. C. Sun, X. R. Zhou, M. Cai, X. L. Sun, *J. Phys. Chem. C* **2007**, *111*, 9130–9135.
[33] T. P. Kumar, R. Ramesh, Y. Y. Lin, G. T. K. Fey, *Electrochem. Commun.* **2004**, *6*, 520–525.
[34] Y. Wang, J. Y. Lee, *Angew. Chem. Int. Ed.* **2006**, *45*, 7039–7042.
[35] C. Martin, O. Crosnier, R. Retoux, D. Belanger, D. M. Schleich, T. Brousse, *Adv. Funct. Mater.* **2011**, *18*, 3524–3530.
[36] E. Kang, Y. S. Jung, A. S. Cavanagh, G. H. Kim, S. M. George, A. C. Dillon, J. K. Kim, J. Lee, *Adv. Funct. Mater.* **2011**, *13*, 2430–2438.
[37] A. V. Murugan, T. Muraliganth, A. Manthiram, *Chem. Mater.* **2009**, *21*, 5004–5006.
[38] E. Kang, Y. S. Jung, G. H. Kim, J. Chun, U. Wiesner, A. C. Dillon, J. K. Kim, J. Lee, *Adv. Funct. Mater.* **2011**, *22*, 4349–4357.